Check for updates

ASME Journal of Solar Energy Engineering
Online journal at:
https://asmedigitalcollection.asme.org/solarenergyengineering

Krutika Appaswamy[1]
School of Mechanical Engineering,
Purdue University,
West Lafayette, IN 47907
e-mail: kappaswa@purdue.edu

Jason Schirck
School of Mechanical Engineering,
Purdue University,
West Lafayette, IN 47907
e-mail: jschirck@purdue.edu

Chathusha Punchi Wedikkara
School of Mechanical Engineering,
Purdue University,
West Lafayette, IN 47907
e-mail: ppunchiw@purdue.edu

Aaron Morris
School of Mechanical Engineering,
Purdue University,
West Lafayette, IN 47907
e-mail: morri353@purdue.edu

Zhiwen Ma
National Renewable Energy Laboratory,
Golden, CO 80401
e-mail: Zhiwen.Ma@nrel.gov

Two-Fluid and Discrete Element Modeling of a Parallel Plate Fluidized Bed Heat Exchanger for Concentrating Solar Power

A novel high-temperature particle solar receiver is developed using a light trapping planar cavity configuration. As particles fall through the cavity, the concentrated solar radiation warms the boundaries of the receiver and in turn heats the particles. Particles flow through the system, forming a fluidized bed at the lower section, leaving the system from the bottom at a constant flowrate. Air is introduced to the system as the fluidizing medium to improve particle heat transfer and mixing. A laboratory scale cavity receiver is built by collaborators at the Colorado School of Mines and their data are used for model validation. In this experimental setup, near IR quartz lamp is used to provide flux to the vertical wall of the heat exchanger. The system is modeled using the discrete element method and a continuum two-fluid method. The computational model matches the experimental system size and the particle size distribution is assumed monodisperse. A new continuum conduction model that accounts for the effects of solid concentration is implemented, and the heat flux boundary condition matches the experimental setup. Radiative heat transfer is estimated using a widely used correlation during the post-processing step to determine an overall heat transfer coefficient. The model is validated against testing data and achieves less than 30% discrepancy and a heat transfer coefficient greater than $1000\,W/m^2\,K$. [DOI: 10.1115/1.4065334]

Keywords: concentrating solar power, TFM, fluidized bed, heat exchanger, DEM

1 Introduction

Concentrating solar power has been shown to be a promising source of continuous, dispatchable renewable energy, especially when combined with thermal energy storage (TES) systems [1,2]. TES traditionally works on the principle of heating a storage media in the charging phase and discharging that heat when needed to ensure a more consistent supply of energy [3,4]. Previous approaches for TES include using molten salts which circulate through the solar receiver where they absorb the concentrated solar radiation in the form of heat during the charging cycle and flow through heat exchangers for power generation in the discharging cycle [5]. Though molten salts have been shown to be an effective heat transfer medium, such salts can become chemically unstable at high temperatures and can also become corrosive [6]. In recent years, high operating temperature particle receivers have been designed. The main benefits of particle receivers are that the particulates are relatively inexpensive, and that the receivers can operate at high temperatures, enabling high thermodynamic efficiencies [7]. Particle receivers of various configurations such as cyclonic, rotary, and free falling as well as with fixed or fluidized bed configurations have been developed, each with their own unique set of benefits [8,9,3]. Lately, Brayton cycles have been shown to be more efficient than the traditionally used Rankine cycle. As a result of this, moving bed heat exchangers have become ubiquitous in systems where particles are used for thermal energy storage. Moving packed bed supercritical carbon dioxide heat exchangers have gained significant popularity due to the significant increase in efficiency of the sCO_2 power cycles or recompression closed Brayton cycles [10,11]. Studies have shown that bubbling fluidized bed heat exchangers help obtain a significantly higher heat transfer coefficient as compared to moving packed beds [11]. In this study, we look at an inert solid particle receiver where the particles are used as the TES media and are directly heated in the receiver cavity by the concentrated solar radiation.

The National Renewable Energy Laboratory (NREL) is developing a high-temperature particle solar receiver using a light trapping planar cavity solar configuration. The receiver design consists of an array of light trapping receiver cavities arranged in the form of a cylinder. Light enters the receiver tower system, concentrated by a heliostat field, and gets trapped within the cavity. This geometry has been shown to have high thermal efficiencies with low

[1]Corresponding author.

Contributed by the Solar Energy Division of ASME for publication in the Journal of Solar Energy Engineering: Including Wind Energy and Building Energy Conservation. Manuscript received September 12, 2023; final manuscript received April 9, 2024; published online May 3, 2024. Assoc. Editor: Luke J. Venstrom.

This work is in part a work of the U.S. Government. ASME disclaims all interest in the U.S. Government's contributions.

Downloaded from http://asmedigitalcollection.asme.org/solarenergyengineering/article-pdf/146/5/051005/7332294/sol_146_5_051005.pdf by guest on 14 October 2024

reradiation losses. The planar cavity concept proposed for high-temperature operations and high thermal efficiencies of the receiver has been described by Ma and Martinek [12]. As mentioned, the particles are indirectly heated as they fall through the receiver cavity and are used as the TES medium. This heating process is integral to the performance of the receiver and hence significant testing and modeling efforts have been allocated to optimize the performance of this heat exchanger. The flow of the particles is gravity driven in the net downward direction at a fixed flowrate through the receiver cavity. A fluidized bed forms within the receiver cavity, which helps the wall to particle heat transfer by increasing the residence time and the mixing.

This study focuses on the development and validation of a computational fluid dynamics (CFD) model of the heat exchanger. The model is calibrated and validated against experimental data using a relatively novel approach. The aim of the model is to elucidate the heat transfer and fluid dynamics in the system and help optimize the performance of the receiver. There are two main motivations to conduct these simulations: (i) to study the particle and gas counterflow motion and study the effect of varying the particle or airflow rate on the heat transfer coefficient and (ii) to enhance the heat transfer.

This study follows the following structure:

- Model details
  —Two-fluid model (TFM)
  —Discrete element modeling (DEM)
- Details of the experimental system modeled
  —Batch mode: used for validation with HSP 40/70 Carbobead particles
  —Continuous mode: counterflow between air and particles with silica sand
- Model validation: batch mode
  —DEM validated against experimental data
  —Nusselt number correlation by Morris et al. [13] against validated DEM model
  —Two-fluid model using the Nusselt number correlation tuned to match experimental data
- Observations, results, and parametric study: continuous mode

Table 1 Governing equations in the continuum model

Continuity equations

Gas:

$$\frac{\partial(\varepsilon_g\rho_g)}{\partial t}+\mathbf{v_g}\cdot\nabla(\varepsilon_g\rho_g)=0$$

Solid:

$$\frac{\partial(\varepsilon_s\rho_s)}{\partial t}+\mathbf{v_s}\cdot\nabla(\varepsilon_s\rho_s)=0$$

Momentum equations

Gas:

$$\frac{\partial(\varepsilon_g\rho_g\mathbf{v_g})}{\partial t}+\nabla\cdot(\varepsilon_g\rho_g\mathbf{v_g}\mathbf{v_g})=-\varepsilon_g\nabla P_g+\nabla\cdot\bar{\bar{\tau}}_g-\beta_{g,s}(\mathbf{v_s}-\mathbf{v_g})-\varepsilon_g\rho_g\mathbf{g}$$

Solid:

$$\frac{\partial(\varepsilon_s\rho_s\mathbf{v_s})}{\partial t}+\nabla\cdot(\varepsilon_s\rho_s\mathbf{v_s}\mathbf{v_s})=-\varepsilon_s\nabla P_s+\nabla\cdot\bar{\bar{\tau}}_s-\beta_{g,s}(\mathbf{v_s}-\mathbf{v_g})+\varepsilon_s\rho_s\mathbf{g}$$

Energy equations

Gas:

$$\frac{\partial(\varepsilon_g\rho_g C_{p,g}T_g)}{\partial t}+\mathbf{v_g}\cdot\nabla(\varepsilon_g\rho_g C_{p,g}T_g)=-\nabla\cdot\mathbf{q_g}-H_g(T_g-T_s)$$

Solid:

$$\frac{\partial(\varepsilon_s\rho_s C_{p,s}T_s)}{\partial t}+\mathbf{v_s}\cdot\nabla(\varepsilon_s\rho_s C_{p,s}T_s)=-\nabla\cdot\mathbf{q_s}+H_g(T_g-T_s)$$

Interphase heat transfer

$$H_g=\frac{6\kappa_g\varepsilon_s\mathrm{Nu}_{gs}}{d_p^2}\mathrm{Nu}_{gs}=\left(7-10\varepsilon_g+5\varepsilon_g^2\right)\left(1+0.7\mathrm{Re}^{0.2}\mathrm{Pr}^{1/3}\right)+\left(1.33-2.4\varepsilon_g+1.2\varepsilon_g^2\right)\mathrm{Re}^{0.7}\mathrm{Pr}^{1/3}\quad[15]$$

2 Methods

2.1 Computational Details. Multiphase flow with interphase exchange, MFiX, an open source CFD code for multiphase flows, is used as the modeling framework for the simulations. The TFM [14] is used to model the particle and air counterflow heat exchanger portion of the receiver, as well as the multiphase heat transfer in the system. The TFM is an Eulerian–Eulerian model, i.e., both the fluid as well as the particles are modeled as interpenetrating continuum fluids [14]. Since the solid particles are not individually tracked, the model is computationally inexpensive, but requires closures for the constitutive relations that dictate the solid stresses and heat flux [13]. The governing equations for mass, momentum, and energy that are solved numerically are shown in Table 1. The equations in Table 1 are obtained from the MFiX theory guide [14].

A model for solid shear developed by Johnson and Jackson [16] is used to describe the "solid shear" which transitions between the plastic and viscous regimes at a critical packing fraction. The Gidaspow drag model [17] is used to model fluid–solid momentum interactions.

The fluid–solid heat transfer is considered to be a function of the temperature difference between the particulate and gas phases as well as the solid concentration. The Gunn correlation for Nusselt number [15] is used, and is valid for a large range of porosity (0.35–1.0) and Reynolds numbers ($\leq 10^5$) [15]. The conductive heat flux for individual phases are implemented by Fourier's law. For the fluid phase

$$\vec{q_g}=-\varepsilon_g\kappa_g\nabla T_g \tag{1}$$

Similarly, for the solid phase

$$\vec{q_s}=-\varepsilon_s\kappa_s\nabla T_s \tag{2}$$

The thermal conductivity of fluids is calculated using

$$\kappa_g=\kappa_{g,\mathrm{ref}}\sqrt{\frac{T_g}{T_{\mathrm{ref}}}} \tag{3}$$

To obtain an effective solid conductivity (κ_s), a continuum conduction model developed by Morris et al. [13] is implemented. The model by Morris et al. [13] uses DEM data to obtain a Nusselt number correlation. This correlation is a function of solid concentration which significantly affects particle-wall heat transfer. Solid conductivity is calculated as a factor of the product of the calculated Nusselt number and gas conductivity in each cell. This effective solid conductivity is then used to implement a constant flux boundary condition for fluidized beds to include the effect of solid concentration on the heat transfer. The idea of using the near-wall conditions and applying it to the bulk of the particle flow [18] has been extended to fluidized beds, with the inclusion of solid fraction being a parameter in calculating the effective conductivity as calculated by Morris correlation. The Nusselt number correlation is valid for a large range of solid concentrations and is given as

$$\frac{\mathrm{Nu}}{\mathrm{Nu}_{\max}}=c_0+c_1\varepsilon+c_2\varepsilon^2+c_3\varepsilon^3+c_4\varepsilon^4+c_5\varepsilon^5+c_6\varepsilon^6+c_7\varepsilon^7 \tag{4}$$

where the coefficients are

$$c_0=1.0830\times10^{-3},\quad c_1=-2.17\times10^{-2}$$
$$c_2=2.4268\times10^{0},\quad c_3=1.9101\times10^{0}$$
$$c_4=-1.2243\times10^{2},\quad c_5=6.1540\times10^{2}$$
$$c_6=-1.1706\times10^{3},\quad c_7=7.9093\times10^{2}$$

The definition of the Nusselt number in Eq. (4) is given as $\mathrm{Nu}=h_{pfw}d_p/\kappa_g$, where $h_{pfw}=q_s''/\Delta T_s$, and ΔT_s is the temperature difference between the wall and the nearby particles in contact with the wall. Morris et al. [13] derive $\mathrm{Nu}_{\max}$ for a single particle analytically accounting for maximum conduction between particles, particle-wall, and through a fluid lens. This $\mathrm{Nu}_{\max}$ depends on the

Downloaded from http://asmedigitalcollection.asme.org/solarenergyengineering/article-pdf/146/5/051005/7332294/sol_146_5_051005.pdf by guest on 14 October 2024

particle size, surface roughness, and the conduction lens radius. From the one-dimensional Fourier's law, we find, $q_s'' = \kappa_s \nabla T_s = \kappa_s(\Delta T_s/\Delta x)$, and on rearranging we get $\kappa_s = \left[\Delta x/d_p\right]\kappa_g \mathrm{Nu}$ or $\kappa_s = C\kappa_g\ \mathrm{Nu}(\varepsilon_s)$ where C is a constant. An acceptable value for C would be close to $1/\mathrm{Bi} \approx 2$ [13] and hence:

$$\kappa_s = 2\kappa_g \mathrm{Nu} \tag{5}$$

By default, MFIX implements a constant heat flux boundary by assuming uniform thermal conductivity of the solid phase and imposing a constant wall normal temperature gradient. In our new model, the thermal conductivity of the solid phase now depends on the concentration field, and MFIX was modified to include such effects. The constant heat flux boundary condition for the two-fluid model in MFiX, for a more accurate boundary heat flux, is modified to

$$q_s'' = \kappa_s \frac{\Delta T_s}{\Delta x/2} \tag{6}$$

where Δx is the cell size in the wall normal direction.

Radiation heat transfer is not directly simulated. Since we operate in temperature regimes where radiation plays a non-negligible role, a correlation by Chen et al. [19] is used while post-processing the data to account for radiation. This correlation is shown in Eq. (8). The correlation captures the wall-to-bed radiation contribution to the overall heat transfer coefficient. It is an approximation of the overall contribution of radiation since wall to bed is the dominant source of radiative exchange in the system. The interparticle radiative exchange is much smaller since in the timescales simulated, the bed temperatures are almost homogeneous.

$$h_{\mathrm{total}} = h_c + h_r \tag{7}$$

$$h_r = \sigma \frac{\left(T_w^4 - \bar{T}_p^{\,4}\right)}{\left(T_w - \bar{T}_p\right)\left(1 + ((1-e_w)/e_w) + ((1-e_p)/e_p)\right)} \tag{8}$$

$$e_w = e_p = 0.85$$

The variables e_w and e_p are the emissivity coefficients of the wall and particle cluster, respectively. A median value from the acceptable range [20] is chosen, and this value affects the heat transfer coefficient by $\pm 30\ \mathrm{W/m^2\,K}$.

The continuum conduction model developed by Morris et al. [13] was developed for moving beds and gravity-assisted chute flows. To test the validity of this Nusselt number correlation for fluidized beds and heat transfer from a vertical wall, DEM is performed for bubbling fluidized beds. DEM is an Eulerian–Lagrangian method where the fluid is modeled as a continuum media similar to the TFM while the solid phase is studied as discrete particles and their motions and momenta are individually tracked. MFiX-DEM is used as a solver for the simulations. The solid phase collisions are resolved using the soft sphere approach which is a kind of a spring-dashpot model [21]. The particle spring constant is set to 1000 N/m and the particle–particle and particle wall friction are set to 0. The gas and solid phases are fully coupled using interphase coupling equations, the Gidaspow drag model for momentum coupling [17], and the Gunn model for energy coupling [15]. The gas phase equations are solved similar to the continuum model while the solid phase equations are solved by resolving the collisions using Newton's laws of motion. The Rong and Horio [22] model is used for conduction between particles and between particles and walls, through direct contact or more dominantly, via fluid film. Soft sphere corrections are applied by setting Young's modulus to 70 GPa and the Poisson's ratio to 0.17. This thickness of the fluid film around the particle through which conduction occurs is called the lens radius. The minimum conduction distance (s) is a model parameter that can be approximated well as the particle surface roughness. Both the lens radius and the minimum conduction distance have a significant effect on the heat transfer to the particles as shown by Morris et al. [13].

2.2 Test System and Modeling Domain. A heat exchanger test station designed by the Colorado School of Mines and their data are used for the validation of the MFiX models. In this heat exchanger, there is a counterflow in the motion between air and particles. Particles enter the system from the top, form a bed, and traverse in a net downward motion to leave the system from the bottom at a constant flowrate. Air enters the system through a distributor near the bottom of the cavity, and lightly fluidizes the system to aid with the mixing and heat transfer. The air leaves the system from outlets present on the side walls near the top. A near IR quartz lamp provides heat flux to one of the vertical walls. Hence the energy input to the system is through a heated wall. Figure 1 shows the test station along with particle and air flow directions as well as location of thermocouples. Table 2 summarizes the particle properties and model inputs for both batch mode and continuous flow simulations. Particles do not exit the system during batch tests, whereas particles flow at a constant flowrate through the system for continuous mode tests. The experimental data used for model validation was obtained from the researchers at the School of Mines. The data are submitted and in review for publication.

2.3 Batch Mode Testing. For batch mode testing, there is a fixed mass of particles, so the system acts as a fluidized bed with heat addition. Heat flux is incident on one of the vertical walls (front) and the other wall (back) is cooled with fans to keep the overall temperature of the bed quasi-steady and with small thermal gradients. The TFM model is calibrated for one value of constant bed temperature and the calibration is validated using a different bed temperature. The particles are preheated to this bed temperature before starting the experiment and hence in the models, the particles are initialized to have the bed temperature. Particles tested in batch mode are 360 μm HSP 40/70 Carbobeads. The inlet air has the same temperature as the bed and a wide range of fluidization conditions are tested. The experimental data from School of Mines are used for model validation.

A DEM model is setup for batch mode which matches the test station dimensions in the direction of the heat transfer. The particles are monodisperse spheres with diameters equal to the Sauter mean

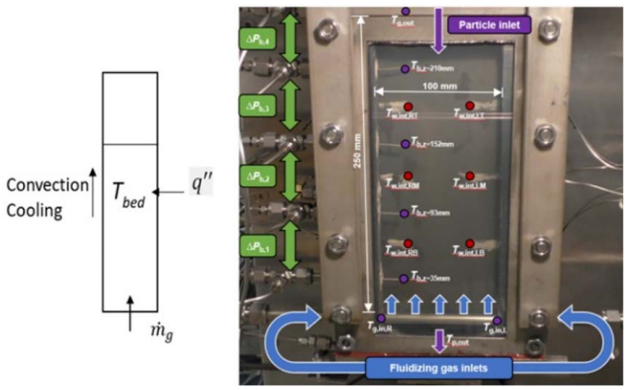

Fig. 1 Schematic of test station. In batch mode, there is no particle inlet or exit. In continuous modes, there is counterflow motion between falling particles and fluidizing air [11].

Table 2 Particle properties for batch and continuous tests

Batch mode	HSP 40/70 (Carbobead)	Continuous mode	Silica sand
d_p	360 μm	d_p	150 μm
ρ_p	3620 kg/m^3	ρ_p	2700 kg/m^3
$C_{p,p}$	1150 J/kg K	$C_{p,p}$	1155 J/kg K
e_p	0.85	e_p	0.85

Downloaded from http://asmedigitalcollection.asme.org/solarenergyengineering/article-pdf/146/5/051005/7332294/sol_146_5_051005.pdf by guest on 14 October 2024

diameter, 360 μm, and the other physical properties are matched. The heated wall is modeled as a constant temperature wall (362 °C for a 300 °C bed bulk temperature) and all other walls are considered to be adiabatic.

Figure 1 shows a schematic of the test station in batch mode. The batch mode test data are used to validate and calibrate both the DEM and TFM conduction models. For the validation of the TFM model, the actual size of the test station ($0.1 \times 0.25 \times 0.012$ m) is simulated to eliminate challenges and uncertainties associated with system scaling. The heat fluxes are matched using the measured flux value as the boundary condition (25 kW/m^2). Convection cooling is modeled using a negative heat flux boundary condition.

2.4 Continuous Mode Simulations. After the model is validated by the batch mode experimental results, TFM simulations with particle flow through the system are performed which mimic the working of the actual receiver cavity. The same dimensions as the School of Mines experimental test station are used. The particle and air counterflow is studied and parametric studies are conducted. Figure 2 shows the computational domain for the counterflow system. The front view is on the far left and shows the initial particle bed and freeboard region. The side view shows the particle bed, freeboard region, and the air outlet (top block on the side view). On the far right, the bottom view is shown followed by the top view of the domain. The bottom includes the air inlet (middle block, bottom view) as well as particle outlets (top and bottom blocks, bottom view) and the top shows the particle inlet (top view). The particles enter the domain from the top ($+y$) surface at a set mass flowrate and leave the domain from a portion of the bottom surface ($-y$). Air enters the domain from the bottom ($-y$), between the two particle outlets, and leaves from the top regions in the $+/-$ x directions. The side walls ($+/-x$) and the back surface ($-z$) are no-slip adiabatic walls.

The front wall ($+z$) acts as the receiver surface and receives a constant heat flux. To aid with maximizing the heat transfer to the particles, smaller 150 μm silica sand particles are tested because reducing the particle size has been shown in the literature to enhance the heat transfer [23]. Note that the continuous simulations are performed with only the two-fluid model.

3 Results and Discussion

3.1 Model Validation

3.1.1 Validation of the Effective Conductivity Model. Since the Nusselt number correlation by Morris et al. [13] was obtained from chute flows, the validity of the model for fluidized beds is tested. For this, the DEM results are validated against the experimental batch mode results and this validated DEM is used to obtain Nusselt numbers to validate the correlation.

The DEM model is setup to match the experimental domain in the direction of heat transfer and is scaled down in the other dimensions to reduce computational expense. The heated wall is set to a constant temperature, which is an average of the observed wall temperature and all other walls are setup as adiabatic boundaries. The time scales of the DEM simulations are quite small so the bed is mostly homogeneous at a temperature equal to the initial bed temperature, which in this case is 300 °C. DEM is performed in batch mode for the 360 μm Carbobead particles.

To validate the DEM models, the simulated heat transfer coefficient is compared to the experimentally obtained values. The heat transfer coefficient (h_{total}) is calculated as the sum of the conductive and convective (h_c) and radiative (h_r) heat transfer coefficients. This heat transfer coefficient is plotted against the ratio of the superficial velocity (u) and minimum fluidization velocity (u_{mf}). This minimum fluidization velocity is the minimum superficial velocity at which the weight of the particle bed is completely supported by the pressure drop of the fluid across the bed and is calculated using the Ergun equation [24].

Figure 3 compares the DEM heat transfer coefficients which are calculated as shown in Eq. (9) with the experiment, validating the model. This validated model is then used to obtain the Nusselt number near the heated wall. The Nusselt number obtained is scaled by the maximum Nusselt number that is obtained similar to the method followed by Morris et al. and plotted against the solid fraction of the cell. The results obtained are compared with the correlation by Morris et al. [13]. This also helps validate the inflow of heat to the system from the heated wall.

Figure 4 shows the comparison of the Nusselt number obtained from the validated DEM simulations and the Nusselt number correlation by Morris et al. [13]. The y axis on the left shows the ratio of the Nusselt number and the maximum Nusselt number and this is plotted against the solid fraction of each near-wall cell. These plots obtained from DEM agree well with the correlation by Morris et al. [13] at more fluidized conditions with small deviations at lesser fluidized cases. This helps validate the solid conductivity model for bubbling beds, which is then used in the two-fluid model.

3.1.2 Validation of the Two-Fluid Model. Validation and tuning of TFM are performed in batch mode for the 360 μm Carbobead particles. For the two-fluid model, similar to DEM, the correlation by Chen et al. [19] shown in Eq. (8) is used for the radiative portion while the conductive and convective contribution is calculated as shown in Eq. (9). Experimentally, the heat transfer coefficient is calculated using the ratio between the flux across the wall and the difference between the wall temperature and the bulk temperature in the middle of the domain in the direction of heat transfer.

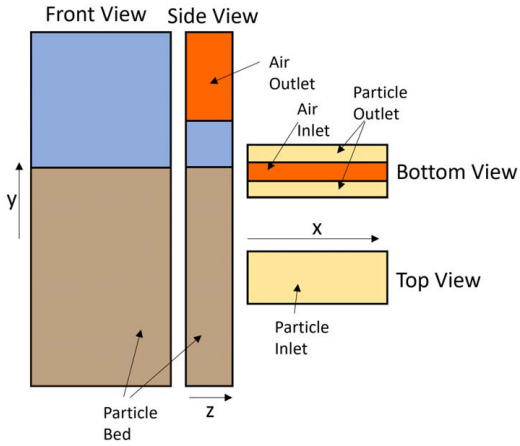

Fig. 2 Computational domain showing the different regions and boundary locations

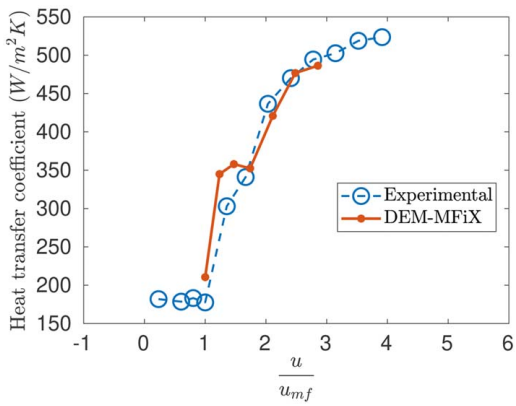

Fig. 3 Validation of DEM against experimental results for 300 °C bed. $d_P = 360\,\mu$m, $T_w = 362$ °C, and inlet air temperature is 300 °C.

Downloaded from http://asmedigitalcollection.asme.org/solarenergyengineering/article-pdf/146/5/051005/7332294/sol_146_5_051005.pdf by guest on 14 October 2024

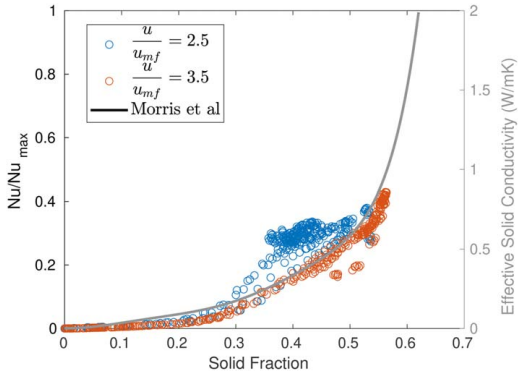

Fig. 4 Validation of Nusselt number correlation against DEM results for bubbling beds at 300 °C. $d_P = 360\,\mu$m, $T_w = 362$ °C, and inlet air temperature is 300 °C.

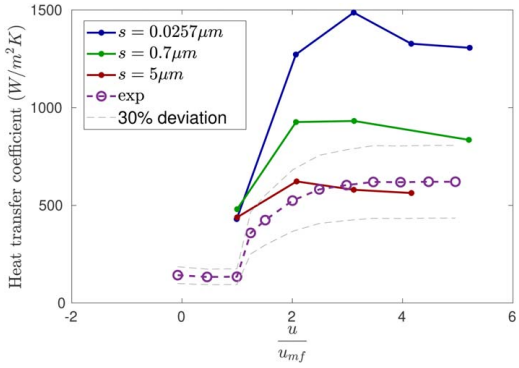

Fig. 5 Calibration of TFM using surface roughness as the calibration parameter. 360 μm particle bed at 500 °C, $q'' = 25{,}000\,\mathrm{W/m^2}$, and air inlet temperature of 500 °C.

Locations of thermocouples, measurements of wall heat flux, particle bulk temperature, and wall temperatures are described by Fosheim et al. [11].

$$h_c = \frac{q''}{(T_w - T_p)} \tag{9}$$

In Eq. (9), q'' is a specified model input in the form of a boundary condition and T_p is the mean particle temperature in the central region of the bed, between the front and back wall, and can be obtained directly from the simulation results. The wall temperature is obtained using near-wall particle temperature and the definition of Nusselt number in terms of gas conductivity and heat transfer coefficient. From the constant flux boundary condition, T_w can be extrapolated as

$$T_w = T_{p,s} + \frac{q''\Delta x}{2\kappa_s} \tag{10}$$

T_p is the particle temperature at the center plane while $T_{p,s}$ is the particle temperature close to the heated wall. To avoid the dependence on the grid size and account for thermal slip at the boundary, we use the definition of Nusselt number:

$$\mathrm{Nu} = \frac{hd_p}{\kappa_g} = \frac{(q''/\Delta T)d_p}{\kappa_g}$$

Rearranging the equation for Nusselt number and replacing $\Delta T = Tw - T_{p,s}$ and $\kappa_s = 2\,\mathrm{Nu}\,\kappa_g$, the wall temperature is

$$T_w = T_{p,s} + \frac{2d_p q''}{\kappa_s} \tag{11}$$

A wide range of fluidization conditions are considered for the model calibration and validation. The heat transfer model requires an input to capture particle roughness effects. Such a roughness coefficient is not directly measured experimentally, so it is used as a model parameter and calibrated with the measured heat transfer data. It is observed that while the model yields the same trends as the experiments with a slight peak in heat transfer coefficient, the heat transfer coefficient is severely overpredicted. The overprediction in the uncalibrated system is due to the assumption that the particles are smooth spheres in the conduction model. Since the real particles will have some roughness, thermal contact would reduce and hence the heat transfer coefficient would reduce. The minimum fluidization velocity, u_{mf}, is defined for the particles at 500 °C using the Ergun equation [24]. The ratio u/u_{mf} helps estimate how fluidized the system is as compared to when it just starts being fluidized. Figure 5 shows the calibration of the model by varying the surface roughness of the particles. Looking at the results, a surface roughness of 5 μm is chosen which is close to the range of measured roughness values for 400 μm particles [25]. This value of surface

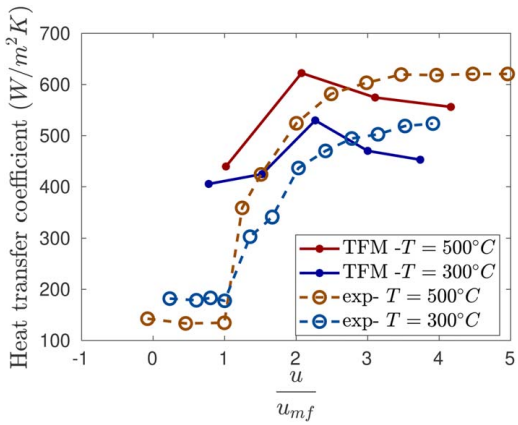

Fig. 6 Validation of calibrated TFM against experimental results at different bed temperatures. 360 μm particle bed and $q'' = 25{,}000\,\mathrm{W/m^2}$.

roughness is then validated by comparing model results obtained to experimental values for a different initial bed temperature, 300 °C, as shown in Fig. 6.

It is important to note that the calibrated model does not perform well in simulating heat transfer in the dense packed bed regime. It is suspected that the reason for this is the hydrodynamic predictions which are a known issue with the continuum model [26,27] and further studies are needed to ensure the validity of the model in those regimes.

3.2 Continuous System With Particle/Air Counterflow. With the complete receiver system, the aim of the simulations is to model the receiver closer to its physical operating conditions and obtain an optimum regime to maximize the heat transfer to the particles. To this effect, smaller particles, silica sand with mean diameter of 150 μm, are tested because the literature shows that reducing particle size generally tends to increase the heat transfer coefficient [23]. These smaller particles are likely what will be used in the actual receiver and hence it is important to study the heat transfer through these particles. It is noted that the model predicted heat transfer coefficient values are likely larger than the actual case because of the assumption of smooth spheres. The actual values would likely be less depending on the surface roughness. Although not shown, simulations were run with the assumption that silica sand has the same surface roughness as the Carbo beads. Heat transfer coefficient values greater than $1000\,\mathrm{W/m^2\,K}$ are obtained for nearly all cases.

Downloaded from http://asmedigitalcollection.asme.org/solarenergyengineering/article-pdf/146/5/051005/7332294/sol_146_5_051005.pdf by guest on 14 October 2024

In the continuous system, heating takes place only from one wall which acts like the receiver wall. Due to this, the region of the bed near the hot wall is generally warmer than the rest of the domain. In these simulations, especially with smaller particles and lower regimes of fluidization, we observe that the gas velocity is higher near the heated wall which indicates a weak channel forms near the wall as shown in Fig. 7. Figure 7 shows the gas velocity contours on the side wall of the domain, where the scale is such that red is a faster $+y$ gas velocity. This channeling reduces the particle concentration near the wall which in turn reduces heat transfer from the wall to the particles. The channeling effect has been attributed to density reduction of air in the warmer regions as compared to the cooler regions. The reduction in density results in a higher gas velocity. Small changes in concentration have a significant effect on the thermal contact, especially as the concentration approaches a packed state. Hence, a proposed solution to eliminate the channeling is to slightly tilt the entire domain toward the heated wall, so that the particles are assisted by gravity to have better thermal contact with the hot wall. The right axis of Fig. 4 also shows how the solid conductivity is affected by the solid concentration.

Regular operating conditions would generally place our solid volume fraction between 0.45 and 0.58 where even slight changes have a significant effect on the effective solid conductivity and hence the heat transfer.

To study the effect of small inclination angles using MFiX simulations, 150 μm silica sand is used, the particle flowrate is kept constant, and the particles enter the system at 750 °C. Air enters the system at a velocity of 0.035 m/s and 750 °C as well. In Fig. 8, it can be seen that even a small inclination significantly helps overcome the channel and improves the heat transfer coefficient.

A parametric study is performed to obtain the optimal particle and airflow rates. To study the air flowrate, 150 μm silica sand is used and once again the particle flowrate is kept constant at 0.024 kg/m^3 and the particles enter the system at 750 °C. For simplicity and to better compare to prior simulations and experimental data, the domain is not inclined. Air enters at 750 °C and the air flowrate is varied. The inlet flux, q'', is kept constant at 200 kW/m^2. Figure 9 shows the results. The minimum fluidization velocity, u_{mf}, is defined for the particles at 750 °C using the Ergun equation [24]. This does not account for the downward motion of air which would change the effective superficial velocity slightly. It can be observed that fluidization significantly improves the mixing in the bed and hence has a large effect on the heat transfer coefficient. The minimum fluidization velocity of the bed is 0.0156 m/s. As the air flowrate increases, a slight peak is observed, similar to the batch mode results. Figure 10 shows that the heat transfer coefficient

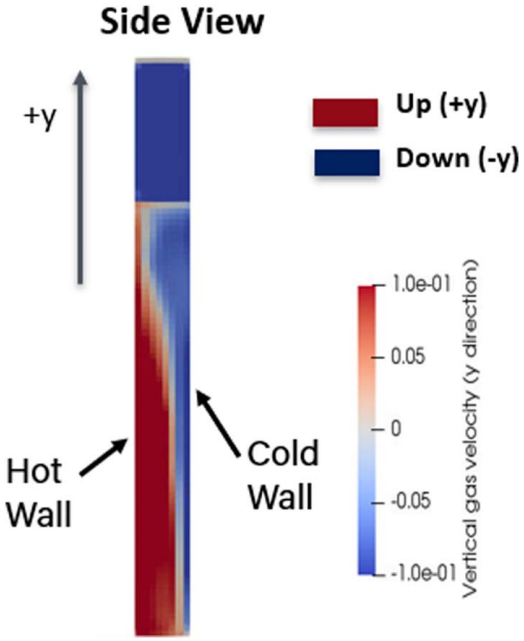

Fig. 7 Vertical (+Y) velocity contours showing gas channeling near heated wall

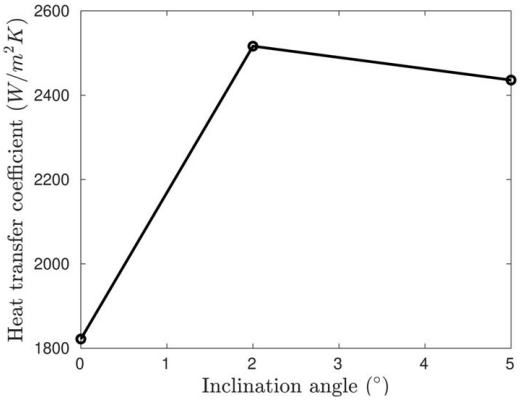

Fig. 8 Increase in heat transfer to the particles due to slight incline of the domain toward the heated wall. 150 μm particles and air enter at 750 °C and the $q'' = 200$ kW/m^2.

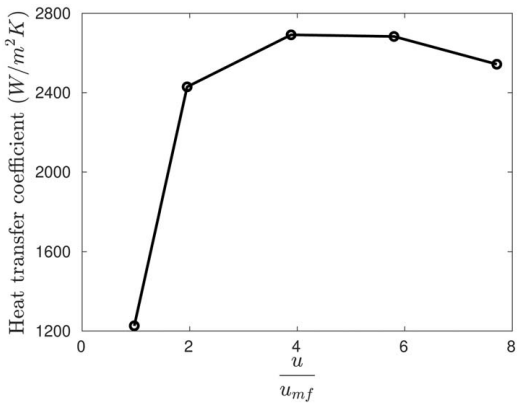

Fig. 9 Increase in heat transfer to the particles due to slight incline of the domain toward the heated wall. 150 μm particles and air enter at 750 °C and the $q'' = 200$ kW/m^2.

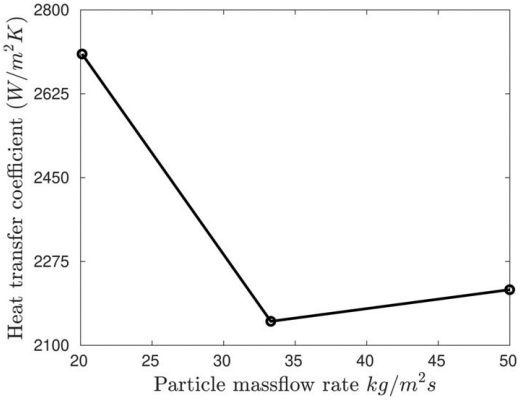

Fig. 10 Effect of particle massflow rate on the heat transfer to the particles. 150 μm particles and air enter at 750 °C and the $q'' = 200$ kW/m^2.

Downloaded from http://asmedigitalcollection.asme.org/solarenergyengineering/article-pdf/146/5/051005/7332294/sol_146_5_051005.pdf by guest on 14 October 2024

reduces as the mass flowrate of particles through the system is increased. This reduction of the heat transfer coefficient for increasing flowrate occurs because the increase in mass flowrate would reduce the residence time of the particles in the heat exchanger. Overall, the configuration of the heat exchanger seems to have good performance with heat transfer coefficients of over a $1000\,\mathrm{W/m^2\,K}$ which puts it well above the industry average and will hence be very effective in improving the receiver efficiency.

4 Conclusion

A high-temperature particle solar receiver is being developed which uses a planar cavity light trapping configuration. A novel narrow channel fluidized bed heat exchanger [11] is being tested to be implemented in the receiver cavity. The heat exchanger has a net gravity-aided downward motion of the particles which are in counterflow against air which acts as a fluidizing medium. This serves the benefit of increasing the residence time of the particles within the heat exchanger as well as mixing the particles for better heat transfer.

A Lagrangian–Eularian (DEM) model was built and validated and then used to validate the solid conduction model. A continuum model is built to simulate this heat exchanger and calibrate against test results. The calibration is conducted by comparing the model heat transfer coefficient to experimentally obtained values and the surface roughness of the particles is varied from completely smooth to a more realistic value. The calibrated model is then validated with a different set of experimental results. The calibration and validation are performed for batch mode with no particle flow and larger HSP 40/70 particles. Smaller silica sand particles are simulated in the continuous mode to enhance heat transfer to the particles. A few important conclusions can be obtained from the continuous simulations. Even slight differences in solid concentration near the heated wall can significantly affect the heat transfer to the particles. The simulations have a heated wall and hence a region where the density of air reduces causing an increase in air velocity which leads to the formation of a narrow channel near the heated wall. This channel reduces the thermal contact of particles with the heated wall. Using an incline to gravity assist particles toward the heated wall helps significantly increase the heat transfer from the wall to the particles.

Fluidization of the bed helps in better heat transfer but increasing the amount of fluidization does not make much difference to the heat transfer until the slugging stage is reached when the heat transfer reduces due to large bubbles. A lower particle flowrate leads to more heated particles as a direct result of the residence time of the particles within the system.

Acknowledgment

The authors acknowledge individuals, institutions, or companies that supported them in preparing the work. Those mentioned might have provided technical support, insightful comments, or conversations, materials used in the work, or access to facilities.

Funding Data

- This work was sponsored by the National Renewable Energy Laboratory which is granted by the U.S. Department of Energy award No. DE-EE0038896.

Conflict of Interest

There are no conflicts of interest.

Data Availability Statement

The datasets generated and supporting the findings of this article are obtainable from the corresponding author upon reasonable request.

Nomenclature

Symbols

e = thermal emissivity
$\vec{g}$ = gravity ($\mathrm{m/s^2}$)
h = heat transfer coefficient ($\mathrm{W/m^2\,K}$)
$\vec{q}$ = heat transfer rate (W)
t = time (s)
$\vec{v}$ = velocity vector (m/s)
D = diameter (m)
H = thermal conductance (W/K)
P = pressure (atm)
T = temperature (K or °C)
C_p = specific heat ($J/kg\,K$)
q'' = heat flux ($\mathrm{W/m^2}$)
Nu = Nusselt number
β = gas–solids drag coefficient
ε = volume fraction
κ = thermal conductivity (W/mK)
ρ = density ($\mathrm{kg/m^3}$)
τ = shear stress ($\mathrm{N/m^2}$)

Subscripts

g = gas
p = particle
pfw = particle-fluid-wall
pw = particle-wall
ref = reference
s = solids
w = wall

References

[1] He, Y.-L., Qiu, Y., Wang, K., Yuan, F., Wang, W.-Q., Li, M.-J., and Guo, J.-Q., 2020, "Perspective of Concentrating Solar Power," Energy, **198**, p. 117373.
[2] Martinek, J., and Ma, Z., 2015, "Granular Flow and Heat-Transfer Study in a Near-Blackbody Enclosed Particle Receiver," ASME J. Sol. Energy Eng., **137**(5), p. 051008.
[3] Zhang, H., Baeyens, J., Cáceres, G., Degrève, J., and Lv, Y., 2016, "Thermal Energy Storage: Recent Developments and Practical Aspects," Prog. Energy Combust. Sci., **53**, pp. 1–40.
[4] Tregambi, C., Troiano, M., Montagnaro, F., Solimene, R., and Salatino, P., 2021, "Fluidized Beds for Concentrated Solar Thermal Technologies—A Review," Front. Energy Res., **9**.
[5] Ma, Z., Glatzmaier, G., and Mehos, M., 2014, "Fluidized Bed Technology for Concentrating Solar Power With Thermal Energy Storage," ASME J. Sol. Energy Eng., **136**(3), p. 031014.
[6] Ge, Z., Li, Y., Li, D., Sun, Z., Jin, Y., Liu, C., Li, C., Leng, G., and Ding, Y., 2014, "Thermal Energy Storage: Challenges and the Role of Particle Technology," Particuology, **15**, pp. 2–8.
[7] Ho, C. K., 2016, "A Review of High-Temperature Particle Receivers for Concentrating Solar Power," Appl. Therm. Eng., **109**(Part B), pp. 958–969. .
[8] Marxer, D., Furler, P., Scheffe, J., Geerlings, H., Falter, C., Batteiger, V., Sizmann, A., and Steinfeld, A., 2015, "Demonstration of the Entire Production Chain to Renewable Kerosene Via Solar Thermochemical Splitting of H_2O and CO_2," Energy Fuels, **29**(5), pp. 3241–3250.
[9] Koepf, E., Villasmil, W., and Meier, A., 2016, "Pilot-Scale Solar Reactor Operation and Characterization for Fuel Production Via the Zn/ZnO Thermochemical Cycle," Appl. Energy, **165**, pp. 1004–1023.
[10] Yin, J., Zheng, Q., and Zhang, X., 2020, "Heat Transfer Model of a Particle Energy Storage–Based Moving Packed Bed Heat Exchanger," Energy Storage, **2**(1), pp. 2–e113.
[11] Fosheim, J. R., Hernandez, X., Abraham, J., Thompson, A., Jesteadt, B., and Jackson, G. S., 2022, "Narrow-Channel Fluidized Beds for Particle-sCO_2 Heat Exchangers in Next Generation CPS Plants," AIP Conf. Proc., **2445**(1), p. 160007.
[12] Ma, Z., and Martinek, J., 2019, "Analysis of Solar Receiver Performance for Chemical-Looping Integration With a Concentrating Solar Thermal System," ASME J. Sol. Energy Eng., **141**(2), p. 021003.

Downloaded from http://asmedigitalcollection.asme.org/solarenergyengineering/article-pdf/146/5/051005/7332294/sol_146_5_051005.pdf by guest on 14 October 2024

[13] Morris, A., Pannala, S., Ma, Z., and Hrenya, C., 2015, "A Conductive Heat Transfer Model for Particle Flows Over Immersed Surfaces," Int. J. Heat Mass Transfer, **89**, pp. 1277–1289.
[14] Syamlal, M., Rogers, W., and O'Brien, T., 1993, "Mfix Documentation Theory Guide."
[15] Gunn, D., 1978, "Transfer of Heat Or Mass to Particles in Fixed and Fluidised Beds," Int. J. Heat Mass Transfer, **21**(4), pp. 467–476.
[16] Johnson, P. C., and Jackson, R., 1987, "Frictional-Collisional Constitutive Relations for Granular Materials, With Application to Plane Shearing," J. Fluid Mech., **176**, pp. 67–93.
[17] Ding, J., and Gidaspow, D., 1990, "A Bubbling Fluidization Model Using Kinetic Theory of Granular Flow," AIChE J., **36**(4), pp. 523–538.
[18] Molerus, O., 1997, "Heat Transfer in Moving Beds With a Stagnant Interstitial Gas," Int. J. Heat Mass Transfer, **40**(17), pp. 4151–4159.
[19] Chen, J. C., Grace, J. R., and Golriz, M. R., 2005, "Heat Transfer in Fluidized Beds: Design Methods," Powder Technol., **150**(2), pp. 123–132. . Scale-Up in Particle Processing.
[20] Ozkaynak, T. F., and Chen, J. C., 1980, "Emulsion Phase Residence Time and Its Use in Heat Transfer Models in Fluidized Beds," AIChE J., **26**(4), pp. 544–550.
[21] Strack, O., Cundall, P., University of Minnesota, Department of Civil and Mineral Engineering, and NSF (U.S.), 1978, *The Distinct Element Method as a Tool for Research in Granular Media: Report to the National Science Foundation Concerning NSF Grant ENG75-20711*, Vol. 2, Department of Civil and Mineral Engineering, Institute of Technology, University of Minnesota, Minneapolis, MN.
[22] Rong, D., and Horio, M., 1999, "DEM Simulations of Char Combustion in a Fluidized Bed," Second International Conference on CFD in the Minerals and Process Industries, Melbourne, Australia, Dec. 6–8, pp. 65–70.
[23] Molerus, O., 1992, "Heat Transfer in Gas Fluidized Beds Part 2. Dependence of Heat Transfer on Gas Velocity," Powder Technol., **70**(1), pp. 15–20.
[24] Ergun, S., and Orning, A. A., 1949, "Fluid Flow Through Randomly Packed Columns and Fluidized Beds," Ind. Eng. Chem., **41**(6), pp. 1179–1184.
[25] Bagepalli, M. V., Yarrington, J. D., Schrader, A. J., Zhang, Z. M., Ranjan, D., and Loutzenhiser, P. G., 2020, "Measurement of Flow Properties Coupled to Experimental and Numerical Analyses of Dense, Granular Flows for Solar Thermal Energy Storage," Sol. Energy, **207**, pp. 77–90.
[26] Ostermeier, P., DeYoung, S., Vandersickel, A., Gleis, S., and Spliethoff, H., 2019, "Comprehensive Investigation and Comparison of TFM, Densedpm and CFD-DEM for Dense Fluidized Beds," Chem. Eng. Sci., **196**, pp. 291–309.
[27] Adnan, M., Sun, J., Ahmad, N., and Wei, J. J., 2021, "Comparative CFD Modeling of a Bubbling Bed Using a Eulerian–Eulerian Two-Fluid Model (TFM) and a Eulerian-Lagrangian Dense Discrete Phase Model (DDPM)," Powder Technol., **383**, pp. 418–442.

Downloaded from http://asmedigitalcollection.asme.org/solarenergyengineering/article-pdf/146/5/051005/7332294/sol_146_5_051005.pdf by guest on 14 October 2024